Journal of Materials Chemistry A

ROYAL SOCIETY OF CHEMISTRY

PAPER

Check for updates

Cite this: *J. Mater. Chem. A*, 2020, **8**, 18721

A novel molecular descriptor for highly efficient (ϕ_{TADF} > 90%) transition metal TADF Au(III) complexes†

Yu Wang,[a] Qian Peng, *[b] Qi Ou,[a] Shiyun Lin[a] and Zhigang Shuai *[a]

It is generally perceived that a fast reverse intersystem crossing rate of $T_1 \rightarrow S_1$ (k_{risc}) is crucial for efficient organic thermally activated delayed fluorescence (TADF) emitters. Herein, we demonstrate the non-radiative decay rate of $T_1 \rightarrow S_0$ (k_{nr}^T) for transition metal complexes that is even more important. We calculated the interconversion rates among S_0, S_1 and T_1 states for two Au(III)–TADF complexes with triphenylamine (TPA) as a donor moiety but with quite different quantum efficiencies: one with a moderate efficiency of 79% and the other with a high efficiency of 94%, and we found that the former has a much larger k_{risc} ($\sim 10^{10}$ s^{-1}) than the latter ($\sim 10^{7}$ s^{-1}). Such contradictions with the conventional picture are attributed to the relatively large k_{nr}^T ($\sim 10^{6}$ s^{-1}) for the former, leading to an overall lower quantum efficiency. Thus, we propose a novel molecular design descriptor (the triplet non-radiative decay rate k_{nr}^T) for highly efficient transition metal TADF emitters. Further, we find that tetradentate ligand scaffolds with 5-5-6 membered chelate rings could reduce k_{nr}^T to $<10^{5}$ s^{-1} for Au(III)–TADF complexes, thereby achieving quantum efficiencies above 90%. Based on this theoretical guideline, we have proposed nine newly designed Au(III) complexes and predicted their high TADF efficiency.

Received 22nd July 2020
Accepted 26th August 2020

DOI: 10.1039/d0ta07149h

rsc.li/materials-a

Introduction

Materials that exhibit thermally activated delayed fluorescence (TADF) are attractive for electroluminescence due to their 100% attainable internal quantum efficiency (IQE).[1] Within the TADF mechanism, the electro-pumped triplet exciton could be converted to a singlet for fluorescence through reverse intersystem crossing (rISC).[2] The efficiency of rISC is decisive in determining the performance of TADF emitters and is enabled by the small singlet-triplet energy splitting factor (ΔE_{ST}) that can be achieved in donor–acceptor structured molecules, in which charge-transfer (CT) characters dominate the lowest singlet (S_1) and the lowest triplet (T_1) excited states.[3] Meanwhile, a sizable spin–orbit coupling (SOC) between singlet and triplet excited states ($\langle S|\hat{H}_{SOC}|T\rangle$) is indispensable for an efficient rISC.[4] Generally, the SOC in pure organic molecules is very small (typically <1 cm^{-1}),[5] while it is large in transition metal TADF complexes (not large enough for efficient phosphorescence at room temperature as in Ir or Pt complexes) due to the heavy atom effect so that a fast k_{risc} up to 10^{8}–10^{10} s^{-1} could be achieved with a small ΔE_{ST}.[6,7] In this regard, numerous efficient TADF materials containing transition metals, including Cu(I),[8–12] Ag(I),[13,14] Pd(II),[15] Au(I),[6,16] and Au(III),[17,18] have been widely synthesized and characterized owning to their moderate SOC, which is larger than that for pure organic compounds. Larger SOC may facilitate $S_1 \leftrightarrow T_1$ electronic transitions, but they may also lead to fast non-radiative decay rates of $T_1 \rightarrow S_0$ (k_{nr}^T) (Scheme 1). For pure organic compounds, ΔE_{ST} was generally believed to be a TADF descriptor since a small ΔE_{ST} implies a large k_{risc}. However, if we look at the two Au(III)–TADF complexes reported in recent experiments,[17,19] one showed 94% TADF efficiency and $k_{risc} = \sim 10^{7}$ s^{-1}, while the other showed 79% efficiency and $k_{risc} \sim 10^{10}$ s^{-1}, and it is clear that ΔE_{ST}, or

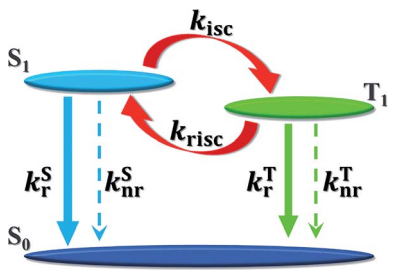

Scheme 1 Excited-state decay and conversion processes including radiative (k_r^S) and non-radiative (k_{nr}^S) decay of $S_1 \rightarrow S_0$, radiative (k_r^T) and non-radiative (k_{nr}^T) decay of $T_1 \rightarrow S_0$, intersystem crossing of $S_1 \rightarrow T_1$ (k_{isc}), and reverse intersystem crossing of $T_1 \rightarrow S_1$ (k_{risc}).

[a]MOE Key Laboratory of Organic OptoElectronics and Molecular Engineering, Department of Chemistry, Tsinghua University, Beijing 100084, P. R. China

[b]CAS Key Laboratory of Organic Solids, Institute of Chemistry, Beijing National Laboratory for Molecular Sciences, Chinese Academy of Sciences, Beijing 100190, P. R. China. E-mail: qpeng@iccas.ac.cn

† Electronic supplementary information (ESI) available: Fig. S1–S8, Chart S1, Tables S1–S10. See DOI: 10.1039/d0ta07149h

k_{risc} is no more a good descriptor. Thus, for transition metal complexes with relatively large SOC, we suggest to use k_{nr}^{T} as a molecular descriptor. The rates involved in TADF (k_r^S, k_{nr}^S, k_r^T, k_{nr}^T, k_{isc}, and k_{risc} in Scheme 1) can be calculated using first-principles *via* the thermal vibration correlation function (TVCF) method that we developed earlier,[20] from which, the overall TADF quantum efficiencies (ϕ_{TADF}) can be evaluated as: $\phi_{TADF} = [\phi_{ISC}\phi_{RISC}/(1 - \phi_{ISC}\phi_{RISC})] \times \phi_F$, where $\phi_{ISC} = k_{isc}/(k_{isc} + k_r^S + k_{nr}^S)$, $\phi_{RISC} = k_{risc}/(k_{risc} + k_r^T + k_{nr}^T)$, and $\phi_F = k_r^S/(k_{isc} + k_r^S + k_{nr}^S)$.[21] Through extensive theoretical studies, we have proposed a molecular design method to reduce k_{nr}^T, based on which we have designed nine Au(III)–TADF complexes, all with $\phi_{TADF} > 90\%$.

Results and discussion

In this study, all density functional theory (DFT) and time-dependent DFT (TDDFT) calculations were performed at the PBE0/6-31g(d, p)/SDD level. Spin–orbit coupling (SOC) calculations for the singlet and triplet states were carried out with the ORCA program.[22] $T_1 \rightarrow S_0$ transition dipole moments were calculated by the Dalton program.[23] More detailed computational approaches can be found in the ESI.†

The skeleton of Au(III)–TADF emitters with a donor (TPA)–acceptor (C^N^C tridentate ligand or C^N^C part of the tetradentate ligand) structure is shown in Chart 1, based on which we carried out the computational study and molecular design. Firstly, we theoretically evaluated complexes **1** and **1L-O** that have been characterized in experiments. The calculated dihedral angle of aryl moieties for complex **1**, as depicted with yellow lines in Chart 1, is 58.84° (experimental value is 53.57°),[17] which is higher than that of **1L-O** (16.63°) owing to its less restrained donor and acceptor moieties. From the natural transition orbital (NTO) analysis in Fig. 1, it can be seen that although both singlet and triplet electronic transitions are dominant with ligand-to-ligand and ligand-to-metal charge transfers (LLCT/LMCT) for the two complexes, **1L-O** has the hole NTOs distribute less on Au–C coordinate bonds and has the electron NTOs distribute more on the aryl moiety of TPA than that on **1**. The calculated fluorescence emission wavelengths for **1** and **1L-O** are 522 nm and 528 nm (experimental observations are 528 nm and 533 nm), respectively. More detailed information

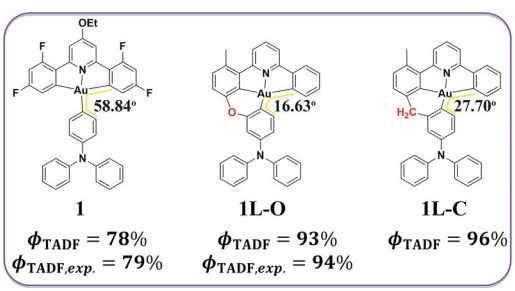

Chart 1 Chemical structures of complex **1** and tetradentate Au(III)–TADF complexes with O (**1L-O**) or C (**1L-C**)-bridged/spiro-arranged ligand scaffolds.

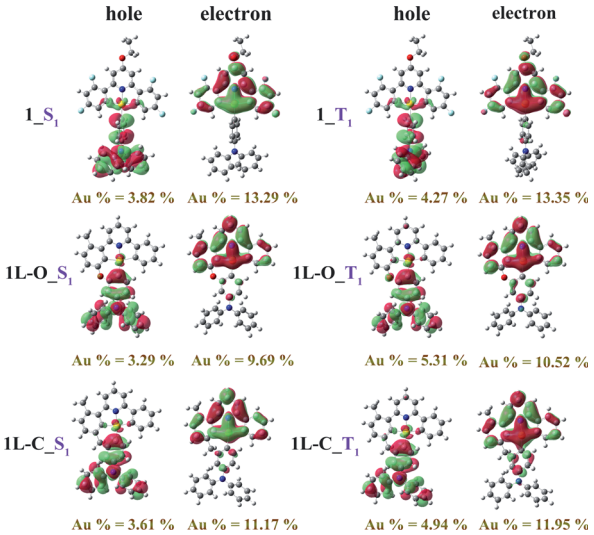

Fig. 1 The hole and electron pairs for $S_1 \rightarrow S_0$ and $T_1 \rightarrow S_0$ transitions obtained by the natural transition orbital (NTO) analysis at optimized S_1 and T_1 geometries of complexes **1**, **1L-O** and **1L-C** (isovalue = 0.02).

on structures and transition properties can be referred in the ESI.†

On the basis of electronic structures obtained from the Gaussian program (see ESI†), interconversion rates are calculated and are listed in Table 1. Herein, only the T_1 state is below the S_1 energy state, and $\Delta E_{T_2S_1}$ is much larger than $\Delta E_{S_1T_1}$, as shown in Fig. S2;† thus, the three-state model shown in Scheme 1 is valid. It can be seen that both k_{isc} and k_{risc} for complex **1** are $\sim 10^{10}$ s^{-1}, and its ϕ_{TADF} is calculated to be 78% (experimental observation is 79% (ref. 17)), indicating the reliability of our TVCF method, which is by the first-principle method without using any empirical parameters. However, this is not as high as expected (over 90% for pure organic emitters). In contrast, ϕ_{TADF} of **1L-O** is 93% (experimental observation is 94%,[19] in good agreement again) but with a calculated $k_{risc} \sim 10^7$ s^{-1}, much lower than **1** but with a higher TADF efficiency. The calculated ΔE_{S1T1} for **1** and **1L-O** are 0.01 and 0.09 eV, respectively. Hence, $\Delta E_{S_1T_1}$ or k_{risc} is no more a good descriptor for these types of TADF emitters. Instead, from Table 1, we note that complex **1** has more than 2 orders of larger magnitude k_{nr}^T than the **1L-O**; therefore, an efficient TADF transition metal complex should have small k_{nr}^T, which could be a novel molecular descriptor.

If we approximate the intersystem crossing rates as $k_{isc} \propto |\langle S|\hat{H}_{SOC}|T\rangle|^2 \exp(-\Delta G)$, where $\Delta G = (-\Delta E_{ST} + \lambda_{ST})^2/4\lambda_{ST}$ (λ_{ST} is the reorganization energy),[24] then for the $T_1 \rightarrow S_0$ non-radiative decay k_{nr}^T, the difference between **1** and **1L-O** is determined largely by $SOC_{S_0T_1}$ and $\lambda_{S_0T_1}$, since the difference in $\Delta E_{S_0T_1}$ is tiny ($\sim$0.1 eV). It is shown in Table 2 that $SOC_{S_0T_1}$ for **1L-O** is about half of that of **1** due to the decrease in the metal Au component in the virtual orbitals involved. This leads to a factor of 4 in k_{nr}^T (square of $SOC_{S_0T_1}$). We note that the difference in k_{nr}^T is about 120 times. Therefore, $\lambda_{S_0T_1}$ is the most responsible factor to account for the drastic reduction of k_{nr}^T. We then analysed the total $\lambda_{S_0T_1}$ of $T_1 \rightarrow S_0$ by decomposing them onto energy relaxation through internal coordinates, as depicted in Fig. 2a–d for

This journal is © The Royal Society of Chemistry 2020

Table 1 Calculated interconversion rates (s^{-1}) among S_0, S_1, and T_1 states, and TADF quantum efficiency (ϕ_{TADF}) for complexes **1**, **1L-O**, and **1L-C**. The $k_{r_{avr.}}$ is calculated by $k_{r_{avr.}} = [3k_r^T + k_r^S \exp(-\Delta E_{S_1T_1}/k_BT)]/[3 + \exp(-\Delta E_{S_1T_1}/k_BT)]$ from ref. 17. The available experimental results are listed in parentheses

	k_r^S ($\times 10^7$)	k_{nr}^S ($\times 10^4$)	k_r^T ($\times 10^3$)	k_{nr}^T ($\times 10^4$)	k_{isc} ($\times 10^8$)	k_{risc} ($\times 10^8$)	$k_{r_{avr.}}$ ($\times 10^5$)	ϕ_{TADF}
1	0.65	3.04	2.75	118	221	147	10.4 (11.1)[a]	0.78 (0.79)[a]
1L-O	3.19	6.60	1.80	0.97	5.05	0.20	2.98 (5.84)[b]	0.93 (0.94)[b]
1L-C	3.33	22.22	1.78	1.62	21.43	0.56	2.73	0.96

[a] Data from ref. 17. [b] Data from ref. 19.

Table 2 Calculated energy gap between S_1 and T_1 states ($\Delta E_{S_1T_1}$), energy barrier of $T_1 \rightarrow S_1$ ($\Delta G_{S_1T_1}$), SOC between S_1/S_0 and T_1 states calculated at optimized T_1 geometries, and reorganization energies (λ) between S_1/S_0 and T_1 states for complexes **1**, **1L-O**, and **1L-C**

	$\Delta E_{S_0T_1}$ (eV)	$SOC_{S_0T_1}$ (cm^{-1})	$\lambda_{S_0T_1}$ (cm^{-1})	$\Delta E_{S_1T_1}$ (eV)	$SOC_{S_1T_1}$ (cm^{-1})	$\lambda_{S_1T_1}$ (cm^{-1})	$\Delta G_{S_1T_1}$ (eV)
1	2.55	186	1676	0.01	4	363	0.02
1L-O	2.43	93	1542	0.09	3	127	0.18
1L-C	2.42	142	1578	0.10	10	73	0.30

1 and **1L-O**. It is revealed from Fig. 2a and c that the $\lambda_{S_0T_1}$ of **1L-O** is 100 cm^{-1}, which is smaller than that of **1** due to the weakened vibronic couplings for low-frequency modes. From Fig. 2b and d, it can be seen that both donors and acceptors contribute primarily to non-radiative decay processes in complex **1**, while for **1L-O** with the O-bridged/spiro-arranged C^C^N^C ligand scaffold, the dominant contributions in $\lambda_{S_0T_1}$ are from the acceptor moiety, without any appreciable contribution from bond/dihedral angles. Thus, we proposed that the tetradentate ligand scaffolds with 5-5-6 membered chelate rings can reduce the vibronic couplings in the TPA moiety; thereby reducing k_{nr}^T to $<10^5$ s^{-1}.

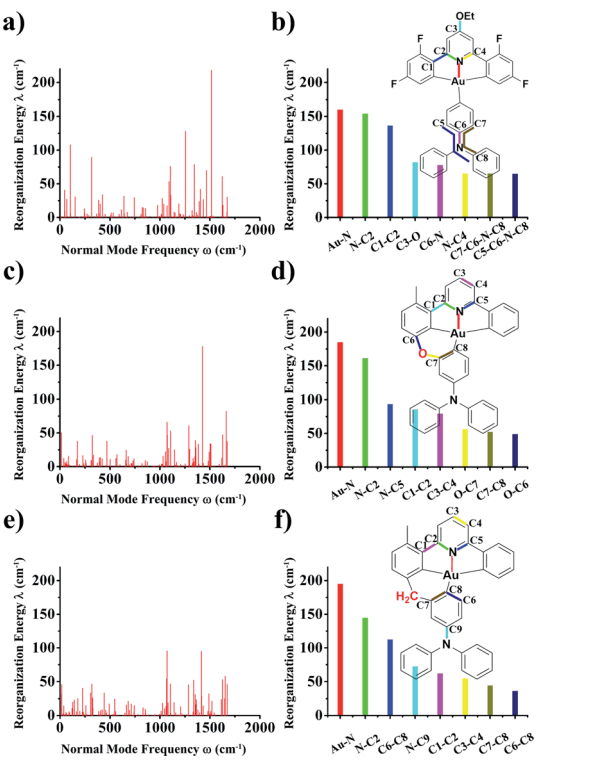

Fig. 2 The $T_1 \rightarrow S_0$ reorganization energies and projections onto the internal coordinates for complexes **1** (a and b), **1L-O** (c and d), and **1L-C** (e and f).

Under such theoretical guidelines, new tetradentate Au(III)–TADF complexes **1L-C** and **1L-N** with C/N-bridged/spiro-arranged C^C^N^C ligand scaffolds are proposed first (Charts 1 and S1†). Nevertheless, **1L-N** is calculated to have quite a low TADF efficiency (ϕ_{TADF} < 0.1%) because its $\Delta E_{S_1T_1}$ is too large (0.28 eV) caused by the large intra-ligand (IL) nature for both S_1 and T_1 states, as shown in Table S4 and Fig. S3.† This means that a small $\Delta E_{S_1T_1}$ is still a prerequisite for TADF, but for molecules with relatively larger SOC, it is not enough.

For **1L-C**, the dihedral angle of aryl moieties, as depicted in Chart 1, is 27.70°, and its electronic transition properties are similar to those of **1L-O**, as shown in Fig. 1. The calculated fluorescence emission wavelength of **1L-C** is 527 nm, as listed in Table S5.† It can be seen from Tables 1 and 2 that with the C-bridged/spiro-arranged tetradentate ligand scaffold, the k_{nr}^T of **1L-C** reduced to $\sim 10^4$ s^{-1}, resulting in an elevated ϕ_{TADF} to 96%, although its k_{risc} is 2 orders of magnitude smaller than that of the complex **1**. Additionally, the $S_1 \rightarrow S_0$ non-radiative decay

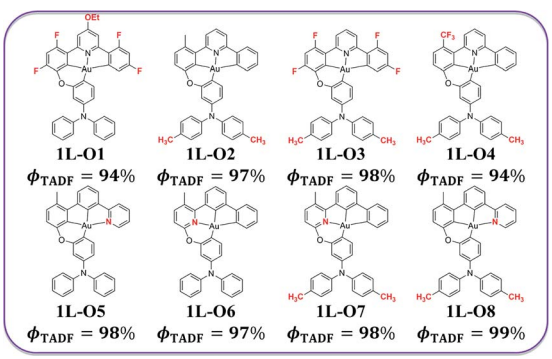

Chart 2 Chemical structures of complexes **1L-O1**–**1L-O8**.

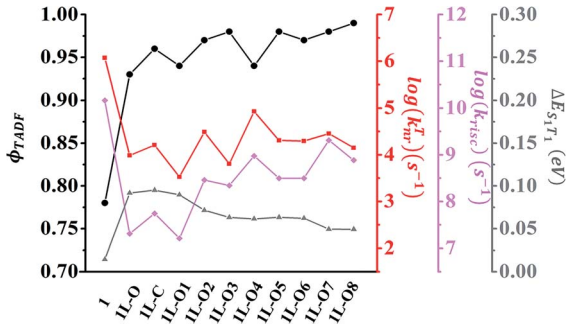

Fig. 3 Line graphs of ϕ_{TADF}, $\log(k_{nr}^{T})$, $\log(k_{isc})$, and $\Delta E_{S_1T_1}$ values for all complexes investigated in this study.

rate (k_{nr}^{S}) is increased by less than one order of magnitude for **1L-C**, which is due to the slightly increased non-adiabatic coupling (NAC), as shown in Fig. S5.† However, main channels of $S_1 \rightarrow S_0$ non-radiative decay among complexes **1**, **1L-O** and **1L-C** are similar, as shown in Fig. S6.†

We have demonstrated above that for efficient transition metal TADF emitters with relatively large SOC, only a small $\Delta E_{S_1T_1}$ is not enough. Instead, a low k_{nr}^{T} should come first. Based on the frame of **1L-O** complexes, we designed a series of complexes **1L-O1–1L-O8**, as shown in Chart 2. The predicted TADF efficiencies range from 94% to 99%. This is because of the separation of the hole and electron NTOs through the addition of electron-withdrawing (electron-donating) groups on acceptor (donor) moieties as well as through the shifting of the position of the pyridine ring within the tetradentate ligand that become C^C^C^N and C^N^C^C ligand scaffolds, thereby decreasing $\Delta E_{S_1T_1}$ while keeping k_{nr}^{T} small (Fig. 3). Expectedly, k_{nr}^{T} of these complexes is all $<10^5$ s^{-1}, and k_{risc} is comparable to or larger than that of **1L-O**. The relevant rates are listed in Table S8.† We stress that **1L-O8** possesses a ϕ_{TADF} of up to 99%.

Conclusions

In summary, we proposed the lowest triplet non-radiative decay rate (k_{nr}^{T}) that should serve as a novel molecular descriptor for highly efficient transition metal TADF complexes from our credible DFT/TDDFT/TVCF calculations. From our theoretical evaluations of two Au(III)–TADF complexes with a TPA donor, the one with sizable $k_{risc} \sim 10^{10}$ s^{-1} has a lower ϕ_{TADF} of 79% than the other with much smaller $k_{risc} \sim 10^{7}$ s^{-1} and higher ϕ_{TADF} of 94%, which is due to more than 2 orders of magnitude larger k_{nr}^{T} of the former than the latter. Therefore, for efficient transition metal TADF emitters with relatively large SOC, $\Delta E_{S_1T_1}$ or k_{risc} is no more a good descriptor as for pure organic TADF emitters. Instead, a slow k_{nr}^{T} is more important. To suppress k_{nr}^{T} in Au(III)–TADF complexes with a TPA donor, employing O/C-bridged tetradentate ligand scaffolds is effective in which $SOC_{S_0T_1}$ and electron-vibration coupling in the TPA moiety are markedly decreased, and ϕ_{TADF} are lifted up to >90%. Impressively, among the nine theoretically designed Au(III)–TADF complexes, **1L-O8** is found to demonstrate a TADF quantum efficiency of 99%. Given the importance of the TADF molecules in the field of OLEDs, we believe the theoretical investigations presented in this communication can serve as guidance to both theoretical and experimental works in the future.

Conflicts of interest

There are no conflicts of interest to declare.

Acknowledgements

This work is supported by the National Natural Science Foundation of China (Grant No. 21788102 and 21973099), the Ministry of Science and Technology of China (Grant No. 2017YFA0204501), and the Strategic Priority Research Program of the Chinese Academy of Sciences (Grant No. XDB12020200).

Notes and references

1 H. Uoyama, K. Goushi, K. Shizu, H. Nomura and C. Adachi, *Nature*, 2012, **492**, 234–238.
2 X.-K. Chen, D. Kim and J.-L. Brédas, *Acc. Chem. Res.*, 2018, **51**, 2215–2224.
3 Q. Zhang, B. Li, S. Huang, H. Nomura, H. Tanaka and C. Adachi, *Nat. Photonics*, 2014, **8**, 326–332.
4 P. de Silva, C. A. Kim, T. Zhu and T. Van Voorhis, *Chem. Mater.*, 2019, **31**, 6995–7006.
5 M. K. Etherington, J. Gibson, H. F. Higginbotham, T. J. Penfold and A. P. Monkman, *Nat. Commun.*, 2016, **7**, 13680.
6 T. Li, D. S. Muthiah Ravinson, R. Haiges, P. I. Djurovich and M. E. Thompson, *J. Am. Chem. Soc.*, 2020, **142**, 6158–6172.
7 D. S. M. Ravinson and M. E. Thompson, *Mater. Horiz.*, 2020, **7**, 1210–1217.
8 T. Hofbeck, U. Monkowius and H. Yersin, *J. Am. Chem. Soc.*, 2015, **137**, 399–404.
9 L. Bergmann, G. J. Hedley, T. Baumann, S. Bräse and I. D. W. Samuel, *Sci. Adv.*, 2016, **2**, e1500889.
10 S. Brown-Xu, M. Fumanal, C. Gourlaouen, L. Gimeno, A. Quatela, C. Thobie-Gautier, E. Blart, A. Planchat, F. Riobé, C. Monnereau, L. X. Chen, C. Daniel and Y. Pellegrin, *Inorg. Chem.*, 2019, **58**, 7730–7745.
11 R. Hamze, J. L. Peltier, D. Sylvinson, M. Jung, J. Cardenas, R. Haiges, M. Soleilhavoup, R. Jazzar, P. I. Djurovich, G. Bertrand and M. E. Thompson, *Science*, 2019, **363**, 601–606.
12 A. Schinabeck, J. Chen, L. Kang, T. Teng, H. H. H. Homeier, A. F. Suleymanova, M. Z. Shafikov, R. Yu, C.-Z. Lu and H. Yersin, *Chem. Mater.*, 2019, **31**, 4392–4404.
13 P. J. Conaghan, S. M. Menke, A. S. Romanov, S. T. E. Jones, A. J. Pearson, E. W. Evans, M. Bochmann, N. C. Greenham and D. Credgington, *Adv. Mater.*, 2018, **30**, 1802285.
14 M. Osawa, H. Yamayoshi, M. Hoshino, Y. Tanaka and M. Akita, *Dalton Trans.*, 2019, **48**, 9094–9103.
15 Z.-Q. Zhu, T. Fleetham, E. Turner and J. Li, *Adv. Mater.*, 2015, **27**, 2533–2537.
16 R. Hamze, S. Shi, S. C. Kapper, D. S. Muthiah Ravinson, L. Estergreen, M.-C. Jung, A. C. Tadle, R. Haiges,

 This journal is © The Royal Society of Chemistry 2020

P. I. Djurovich, J. L. Peltier, R. Jazzar, G. Bertrand, S. E. Bradforth and M. E. Thompson, *J. Am. Chem. Soc.*, 2019, **141**, 8616–8626.
17 W.-P. To, D. Zhou, G. S. M. Tong, G. Cheng, C. Yang and C.-M. Che, *Angew. Chem., Int. Ed.*, 2017, **56**, 14036–14041.
18 D. Zhou, W.-P. To, Y. Kwak, Y. Cho, G. Cheng, G. S. M. Tong and C.-M. Che, *Adv. Sci.*, 2019, **6**, 1802297.
19 D. Zhou, W.-P. To, G. S. M. Tong, G. Cheng, L. Du, D. L. Phillips and C.-M. Che, *Angew. Chem., Int. Ed.*, 2020, **59**, 6375–6382.
20 Q. Peng, Y. Niu, Q. Shi, X. Gao and Z. Shuai, *J. Chem. Theory Comput.*, 2013, **9**, 1132–1143.
21 Q. Peng, D. Fan, R. Duan, Y. Yi, Y. Niu, D. Wang and Z. Shuai, *J. Phys. Chem. C*, 2017, **121**, 13448–13456.
22 F. Neese, *Wiley Interdiscip. Rev.: Comput. Mol. Sci.*, 2012, **2**, 73–78.
23 K. Aidas, C. Angeli, K. L. Bak, V. Bakken, R. Bast, L. Boman, O. Christiansen, R. Cimiraglia, S. Coriani, P. Dahle, E. K. Dalskov, U. Ekström, T. Enevoldsen, J. J. Eriksen, P. Ettenhuber, B. Fernández, L. Ferrighi, H. Fliegl, L. Frediani, K. Hald, A. Halkier, C. Hättig, H. Heiberg, T. Helgaker, A. C. Hennum, H. Hettema, E. Hjertenæs, S. Høst, I.-M. Høyvik, M. F. Iozzi, B. Jansík, H. J. A. Jensen, D. Jonsson, P. Jørgensen, J. Kauczor, S. Kirpekar, T. Kjærgaard, W. Klopper, S. Knecht, R. Kobayashi, H. Koch, J. Kongsted, A. Krapp, K. Kristensen, A. Ligabue, O. B. Lutnæs, J. I. Melo, K. V. Mikkelsen, R. H. Myhre, C. Neiss, C. B. Nielsen, P. Norman, J. Olsen, J. M. H. Olsen, A. Osted, M. J. Packer, F. Pawlowski, T. B. Pedersen, P. F. Provasi, S. Reine, Z. Rinkevicius, T. A. Ruden, K. Ruud, V. V Rybkin, P. Sałek, C. C. M. Samson, A. S. de Merás, T. Saue, S. P. A. Sauer, B. Schimmelpfennig, K. Sneskov, A. H. Steindal, K. O. Sylvester-Hvid, P. R. Taylor, A. M. Teale, E. I. Tellgren, D. P. Tew, A. J. Thorvaldsen, L. Thøgersen, O. Vahtras, M. A. Watson, D. J. D. Wilson, M. Ziolkowski and H. Ågren, *Wiley Interdiscip. Rev.: Comput. Mol. Sci.*, 2014, **4**, 269–284.
24 Z. Shuai and Q. Peng, *Phys. Rep.*, 2014, **537**, 123–156.